nature communications

Article

https://doi.org/10.1038/s41467-026-69115-7

Hierarchical assembly of a Ti_{24} metal-organic polyhedron via kinetic trapping of intermediates

Received: 23 September 2025

Accepted: 20 January 2026

Published online: 03 February 2026

Check for updates

Hui-Zi Li[1,2], Chang-Yin Yang[3], Cheng Gu[4], Fei Wang[1] ✉ & Jian Zhang[1] ✉

The synthesis of high-nuclearity titanium metal-organic polyhedra (Ti-MOPs) has remained a formidable challenge due to the high oxophilicity and hydrolysis susceptibility of Ti^{4+} ions. Herein, we report a Ti_{24} MOP with a truncated octahedron (tro) topology, which represents the highest nuclearity Ti-MOP reported to date. Beyond structural characterization, we introduce a pathway intervention strategy using Ni^{2+} as a kinetic modulator to trap and structurally characterize two key intermediates—a Ti_{12} macrocycle and a Ti_{12} (6-4-6) module. These intermediates outline a hierarchical assembly pathway from simple precursors to Ti_{24} MOP. Furthermore, we demonstrate that this process is governed by a coordination lability gradient between Ti^{4+} and Ni^{2+}, providing an effective strategy for directing supramolecular complexity. This Ti-MOP exhibits permanent microporosity, gas separation, and post-assembly modification capability. This work transforms a synthetic challenge into a strategic advantage, offering a blueprint for the rational assembly of complex metal-organic architectures.

The programmable construction of metal-organic polyhedra (MOPs) represents a central goal in supramolecular chemistry[1–7], driven by their potential for creating tailored nanocavities with applications in separation, catalysis, and sensing[8–12]. A significant barrier to achieving this goal is the inherent difficulty in probing self-assembly mechanisms, which typically involve high-energy intermediates[13]. While in situ techniques such as nuclear magnetic resonance (NMR)[14,15], high-resolution mass spectrometry (HRMS)[16], and fluorescence spectrum[17] can track coordination processes in real time to some extent, they often lack the structural resolution needed to unambiguously identify intermediate species.

This challenge is particularly acute in titanium chemistry, where the high reactivity and oxophilicity of Ti^{4+} ions[18–20] typically lead to the formation of thermodynamically stable titanium-oxo clusters (TOCs)[21–25] or metal-organic frameworks (Ti-MOFs)[26–30], rather than discrete Ti-MOPs[31–34]. Since Raymond's pioneering report on tetrahedral Ti_4 MOP in 1998[35], although certain progress has been made in this field, there are still fewer than 20 types of Ti-MOPs to date[31]. These structures still have the following limitations: i) low nuclearities (≤18 Ti atoms)[34], ii) simplistic topologies such as tetrahedra and cubes[36–38] (Fig. 1a), and iii) low modifiability. The lack of structural complexity and functional versatility in known Ti-MOPs highlights a significant gap in the field. Although our group has contributed to this area with the synthesis of a giant cage-like Ti_{42} oxo-cluster and several Ti-MOPs[36,39–41], the development of high-nuclearity Ti-MOPs with sophisticated architectures remains a formidable challenge, owing to the difficulty in controlling Ti^{4+} ion reactivity and hydrolysis.

Herein, we have successfully synthesized and determined the crystal structure of FIR-151—a Ti_{24} MOP with tro topology. This high-symmetry cage not only represents the highest nuclearity Ti-MOP reported to date, but also demonstrates how the inherent challenges of titanium coordination chemistry can be overcome to achieve architectural complexity. The assembly pathway was elucidated through the structural characterization of two key intermediates: a Ti_{12}

[1]State Key Laboratory of Structural Chemistry, Fujian Institute of Research on the Structure of Matter, Chinese Academy of Sciences, Fuzhou, Fujian, P. R. China. [2]University of Chinese Academy of Sciences, Chinese Academy of Sciences, Beijing, P. R. China. [3]School of Chemistry and Molecular Engineering, East China Normal University, Shanghai, P. R. China. [4]College of Polymer Science and Engineering, State Key Laboratory of Polymer Materials Engineering, Sichuan University, Chengdu, P. R. China. ✉e-mail: wangfei04@fjirsm.ac.cn; zhj@fjirsm.ac.cn

https://doi.org/10.1038/s41467-026-69115-7

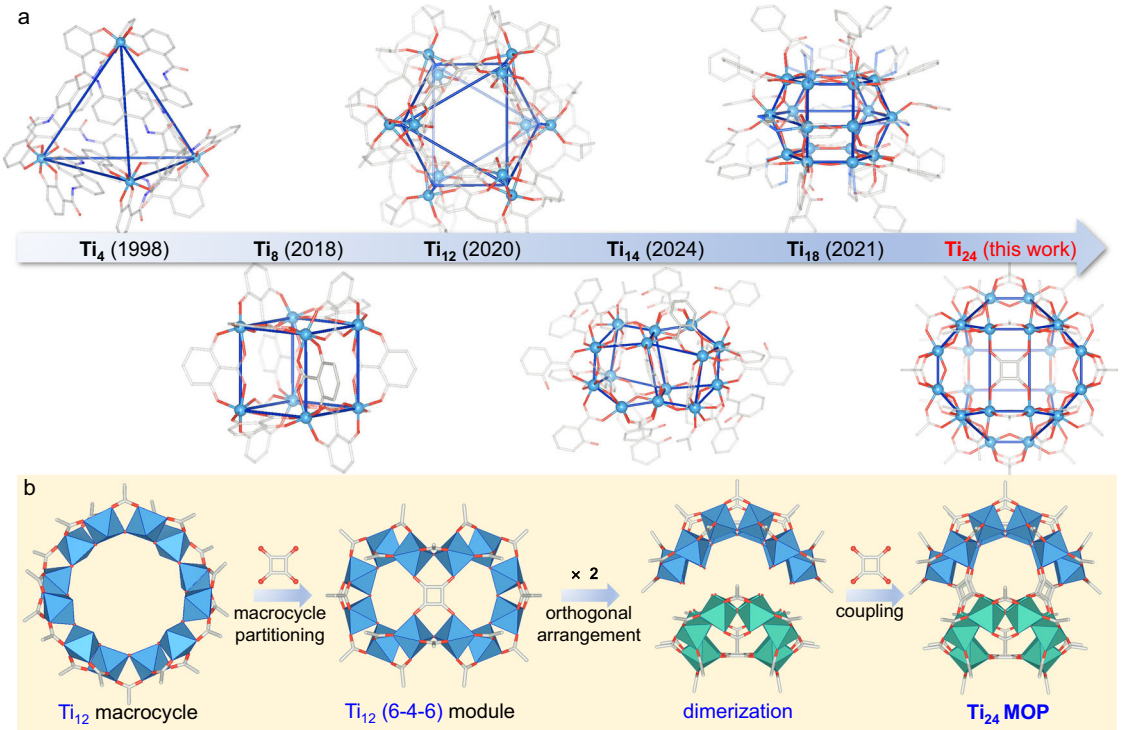

Fig. 1 | Structural evolution and hierarchical assembly of Ti-MOPs. a Crystal structures and publication years of representative Ti-MOPs: Ti_4 (ref. 35), Ti_8 (ref. 38), Ti_{12} (ref. 32), Ti_{14} (ref. 33), Ti_{18} (ref. 34), and Ti_{24} (FIR-151, this work). **b** Proposed hierarchical assembly mechanism of the Ti_{24} MOP, illustrating the stepwise formation from primary building units to the final polyhedral architecture. Atom colors: Ti, sky blue; C, gray; O, red. All hydrogen atoms are omitted for clarity.

macrocycle (FIR-152) and a Ti_{12} (6-4-6) module (FIR-153). These structures provide direct evidence for a hierarchical assembly pathway (Fig. 1b), underpinned by a coordination lability gradient between Ti^{4+} and Ni^{2+}. Furthermore, FIR-151 exhibits permanent porosity, selective gas adsorption, and post-assembly modification capabilities, demonstrating functional relevance. This work not only advances the understanding of titanium supramolecular chemistry but also establishes an effective strategy for achieving programmable synthesis in dynamic metal-organic systems.

Results

Squaric acid ($H_2C_4O_4$) is frequently employed as an organic template to facilitate the ring expansion and assembly of macrocyclic compounds[42]. In existing titanium complexes, it has been observed that the $C_4O_4^{2-}$ ligand coordinates with four Ti^{4+} ions to form a 4-membered ring module[43,44]. Such modules are often found in complex polyhedral structures, exhibiting topological types such as *sod*, *rho*, and *lta*. Here, we select Ti^{4+} ions and $C_4O_4^{2-}$ ligands for assembly to construct polyhedral featuring intricate topological architectures. The reaction of $Ti(O^iPr)_4$ with $H_2C_4O_4$ in the mixture solvent of acetic acid (CH_3COOH)/acetonitrile (CH_3CN) at 120 °C led to the formation of yellow rhombic dodecahedral crystals of FIR-151 (FIR = Fujian Institute Research; Supplementary Fig. 1). Single-crystal X-ray diffraction (SCXRD) analysis reveals that FIR-151 crystallizes in the tetragonal $P4_2/nmc$ space group with the formula as $Ti_{24}O_{24}(C_4O_4)_6(CH_3COO)_{36}$·guest (Supplementary Fig. 2 and Table S1). Its structure features a Ti_{24} MOP with a tro topology, representing the highest nuclearity Ti-MOP reported to date (Fig. 2a).

To elucidate the structure of FIR-151, we conducted a detailed analysis (Supplementary Fig. 3). Firstly, twelve Ti atoms are bridged by twelve μ_2-O atoms to form a Ti_{12} macrocycle—marking what is, to the best of our knowledge, the first observation of such a Ti_{12} structure (Supplementary Table S2). This ring is capped by eighteen terminally coordinated CH_3COO^- ligands. Then, one $C_4O_4^{2-}$ ligand positions within the central pore of the Ti_{12} ring, coordinating to four Ti atoms, leading to the formation of a Ti_{12} (6-4-6) module. Four additional $C_4O_4^{2-}$ ligands occupy the remaining coordination sites on the Ti atoms within this module. The incorporation of $C_4O_4^{2-}$ induces a conformational change in the Ti_{12} macrocycle, causing it to narrow and bend into a distinct roof-like architecture. This contrasts sharply with the planar or S-shaped configurations typically found in other wheel-type TOCs (Supplementary Fig. 4)[25]. The cage structure of FIR-151 can be viewed as a dimer of two Ti_{12} (6-4-6) modules via four shared $C_4O_4^{2-}$ ligands (Fig. 2b and Supplementary Fig. 5). The assembly pathway of FIR-151, involving the dimerization of two curved Ti_{12} (6-4-6) modules, is reminiscent of the formation of iconic supramolecular structures such as the 'tennis ball' capsule[45]. In that system, two identical, curved organic subunits self-assemble through hydrogen bonds to form a closed spheroidal cavity capable of encapsulating guest molecules. The convergence of this geometric design principle across both organic hydrogen-bonded systems and inorganic MOPs underscores its universality for constructing closed-shell nanostructures from pre-organized, curved building blocks. As such, the overall assembly can be topologically represented as a truncated octahedron with the point symbol ($4^6.6^8$) (Fig. 2c). It is noteworthy that the square faces in the topological representation are realized as rectangles in the actual structure; this geometric distortion does not affect the topological classification. To the best of our knowledge, this structure provides an instance of a tro-type topology in Ti-MOP (Supplementary Table S3). The resulting structure measures approximately 18.7 × 18.7 × 20.2 $Å^3$ and features a spherical inner cavity with a diameter of roughly 10.0 Å. Electrostatic potential (ESP) calculations reveal that FIR-151 is electrically neutral overall, yet features negatively charged open windows that favor interaction with cationic guest species (Supplementary Fig. 6). Moreover, these cages adopt a body-centered cubic close-packed arrangement in FIR-151 (Supplementary Fig. 7).

To deconvolute the pathway leading to this MOP, we designed a strategy to perturb the assembly equilibrium using kinetic trappers,

https://doi.org/10.1038/s41467-026-69115-7

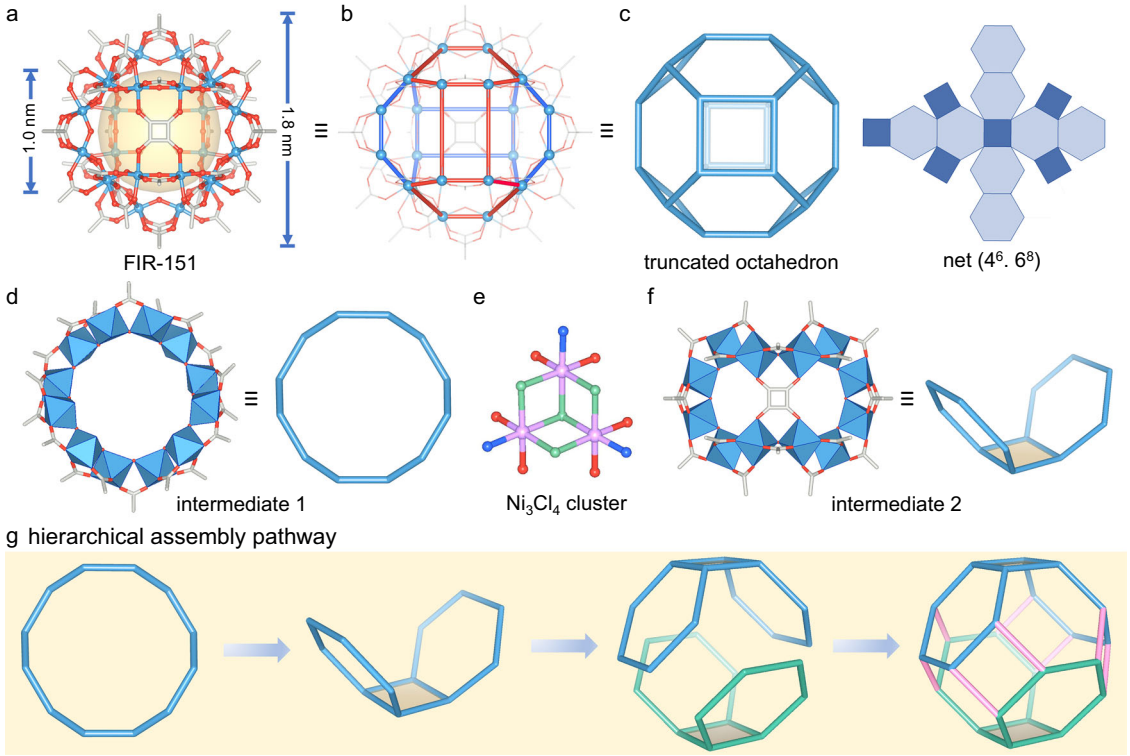

Fig. 2 | Structural and hierarchical assembly of the Ti_{24} MOP and its assembly intermediates. a Molecular structure of FIR-151. **b** Topological representation of FIR-151, with spheres denoting Ti atoms (vertices) and rods representing Ti-Ti edges. The Ti_{12} (6-4-6) module is highlighted in red. **c** Graphical representations of the truncated octahedron and its corresponding net, composed of six squares and eight hexagons. Molecular structures of the intermediate species and kinetic trapper: the Ti_{12} macrocycle (intermediate 1, **d** the Ni_3Cl_4 cluster (kinetic trapper, **e** and Ti_{12} (6-4-6) modular (intermediate 2, **f**). **g** Proposed hierarchical assembly mechanism of the truncated octahedral-type MOP. Atom colors: Ti, sky blue; Ni, purple; C, gray; O, red; Cl, green; N, blue. All hydrogen atoms are omitted for clarity.

aiming to stabilize and isolate metastable intermediates for structural characterization (Supplementary Fig. 8).

Intervention I: Trapping a macrocyclic precursor with Ni^{2+}. Introducing $NiCl_2{\cdot}6H_2O$ into the reaction mixture leads to the isolation of yellow block-shaped crystals of FIR-152 (Supplementary Fig. 9). SCXRD analysis reveals that it crystallizes in the monoclinic space group $P2_1/n$. Its structure is represented by the formula $[Ni(CH_3CN)_6]^{2+}{\cdot}[Ti_{12}Ni_6O_{12}Cl_8(C_4O_4)_6(CH_3COO)_{18}(CH_3CN)_6]^{2-}$ (Supplementary Table S4), and is built around Ti_{12} macrocycle—corresponding to intermediate 1 (Fig. 2d). Two Ni_3Cl_4 clusters are positioned above and below the Ti_{12} macrocycle and are connected to it via three $C_4O_4^{2-}$ ligands, forming a heterometallic MOP, FIR-152. The incorporation of the two Ni_3Cl_4 clusters (Fig. 2e) results in a chair-like configuration of the Ti_{12} macrocycle ring. We propose that Ni^{2+} acts as a kinetic trap for this oligomeric species by modulating the local coordination thermodynamics, thereby stabilizing a critical nucleation intermediate along the assembly pathway.

Intervention II: Directing evolution with quaternary ammonium ions. When tetrabutylammonium bromide (TBAB) was introduced under otherwise identical reaction conditions, a structural rearrangement occurred, leading to the formation of orange hexagonal dipyramid crystals assigned as the isomeric phase FIR-153 (space group *Cmcm*, Supplementary Fig. 10 and Table S4). This compound features a Ti_{12} (6-4-6) modular structure (intermediate 2, Fig. 2f) in which the original 12-membered ring adopts a boat conformation. A central $C_4O_4^{2-}$ ligand partitions the ring via coordination to four Ti^{4+} ions, while two Ni_3Cl_4 clusters reposition to apical sites, linked by additional $C_4O_4^{2-}$ ligands to form an isomeric MOP. Here, Ni^{2+} again serves to kinetically trap this reconfigured module. This transformation demonstrates how non-coordinating additives can profoundly influence the assembly landscape, steering the reorganization of a metastable intermediate into an on-pathway structural motif preceding the final MOP. The molecular structures of both intermediates, FIR-152 and FIR-153, were corroborated in solution by ^1H NMR and small-angle X-ray scattering (SAXS) techniques (Supplementary Figs. 11–14). To elucidate the assembly pathway of FIR-151, we employed a combination of solution-phase, structural, and reactivity analyses. Real-time SAXS monitoring revealed a continuous evolution of the maximum particle dimension (D_{max}), as derived from the pair distance distribution function, $P(r)$, from an initial ~6.7 Å through discrete states (~9.5 Å, ~17.0 Å) to the final ~19.1 Å (Supplementary Fig. 15). This progression is consistent with a multi-step assembly process rather than a single-step reaction. To gain atomic-level insight into potential intermediates along this pathway, we introduced Ni^{2+} ions as a kinetic trap, successfully isolating two key structural modules: the Ti_{12} macrocycle (FIR-152) and the Ti_{12} (6-4-6) module (FIR-153). Their precise structural complementarity provides a plausible geometric model for the progression towards the final cage. Critical reactivity tests further support this interpretation: while FIR-151 forms efficiently in the absence of Ni^{2+}, the Ni^{2+}-stabilized FIR-153 cannot be converted to the final product under identical conditions. This indicates that Ni^{2+} acts to trap and stabilize transient, on-pathway species, which would otherwise be unobservable. While each line of evidence—solution dynamics, structural correlation, and chemical reactivity—has inherent limitations, their convergence mutually supports a coherent, hierarchical assembly pathway from simple precursors to the complex Ti_{24} architecture.

Comparative analysis of the intermediates and the final product with precise crystal structures allows us to propose a hierarchical assembly pathway: Ti_{12} macrocycle (intervention 1) → Reorganization → Ti_{12} (6-4-6) module (intervention 2) → Dimerization → Ti_{24} MOP (Fig. 3a). This mechanistic proposal is best regarded as a robust working hypothesis, substantiated by the convergence of multiple

https://doi.org/10.1038/s41467-026-69115-7

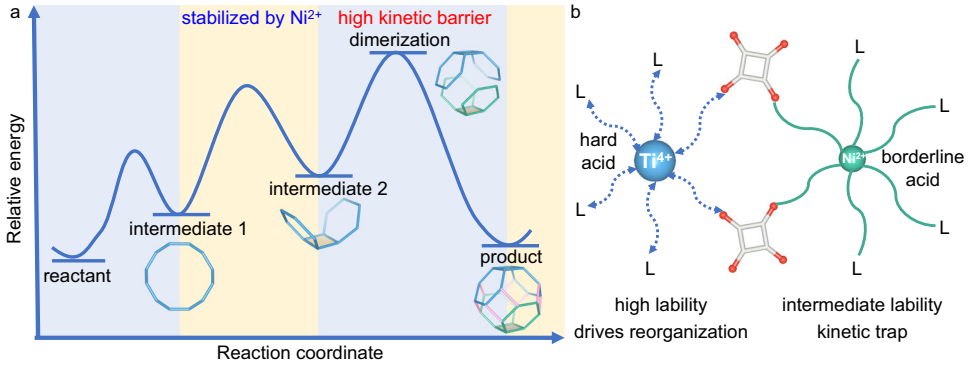

Fig. 3 | Energy landscape and the role of coordination gradient. a A simplified energy landscape of the assembly of the Ti_{24} MOP. The reaction pathway involves i) kinetically trapped intermediates (intermediate 1 and intermediate 2) and ii) a high kinetic barrier corresponding to the dimerization step. The Ni^{2+} ion acts to stabilize the reaction energy, facilitating intermediate capture, while the dynamic nature of the Ti^{4+} ion promotes structural reorganization along the pathway. **b** Coordination lability gradient directs assembly pathway. The Ti^{4+} ion, a hard acid, exhibits high lability with rapidly exchanging coordination bonds (dotted line), driving structural reorganization. In contrast, the borderline acid Ni^{2+} ion displays intermediate lability, forming more stable coordination bonds that act as a kinetic trap and stabilize transient intermediates.

experimental observations within the current technical constraints. We acknowledge that definitive proof would require direct molecular-level tracking of the transient intermediates in solution. Nevertheless, this hypothesis provides a valuable structural and conceptual framework for understanding the complex self-assembly of high-nuclearity MOPs and paves the way for future investigations using advanced in situ techniques.

This work supplies an effective strategy that extends beyond a single case study: the strategic use of coordination lability gradients (Fig. 3b). The assembly is controlled by the differential kinetics between the highly labile Ti^{4+} ion, which drives dynamic reorganization, and the moderately labile Ni^{2+} ion, which acts as a kinetic trap to stabilize key intermediates at defined points along the pathway. This strategy of using a second metal ion to modulate the energy landscape of a primary assembly process offers an alternative approach to achieve structural complexity, and its broad utility awaits validation in other metal-organic systems.

The as-synthesized FIR-151 were further characterized using various analytical techniques to confirm their phase purity, thermal stabilities, optical bandgap, and photoactivity (Supplementary Figs. 16–22). FIR-151 exhibits high stability towards common organic solvents and some acids and bases (Supplementary Fig. 23), enabling investigation of its gas adsorption and separation properties. To evaluate its porosity, the solvent-exchanged sample (CH_3CN) was activated under vacuum at 30 °C for 12 h (Supplementary Fig. 24). N_2-sorption isotherms measured at 77 K revealed a type I isotherm, confirming the microporous nature and permanent porosity of FIR-151 (Fig. 4a). The Brunauer–Emmett–Teller (BET) and Langmuir surface areas were calculated to be 703 and 859 $m^2 \cdot g^{-1}$ (Supplementary Fig. 25), respectively—significantly higher than those of most reported MOPs[2,46]. The total pore volume, estimated from the N_2 uptake at a relative pressure of $P/P_0 = 0.998$, is 0.322 $cm^3 \cdot g^{-1}$ (Supplementary Fig. 26). Density functional theory (DFT) pore size distribution analysis further indicated a predominant pore width of 7.5 Å (Fig. 4b).

Leveraging its high surface area, we further assessed FIR-151's gas separation potential via CO_2, C_2H_2, C_2H_4, and C_2H_6 sorption at 273 and 298 K (Fig. 4c, d, and Supplementary Figs. 27–31). FIR-151 exhibits a high CO_2 uptake capacity of 79 $cm^3 \cdot g^{-1}$ at 273 K and 51 $cm^3 \cdot g^{-1}$ at 298 K, with an isosteric heat of adsorption (Q_{st}) of 40 $kJ \cdot mol^{-1}$, indicating strong host-guest interactions within the pores. Furthermore, FIR-151 shows distinct gas uptake profiles for C_2 hydrocarbons: under identical conditions, sorption capacities for C_2H_2, C_2H_4, and C_2H_6 were measured as 73, 53, and 35 $cm^3 \cdot g^{-1}$ at 273 K, and 60, 38, and 25 $cm^3 \cdot g^{-1}$ at 298 K, respectively. The corresponding Q_{st} values are 32, 28, and 27 $kJ \cdot mol^{-1}$, reflecting differential binding affinities. The notable contrast in both uptake capacity and adsorption enthalpy among these gases underscores the potential of FIR-151 for highly selective gas separation. To quantitatively predict separation selectivity, ideal adsorbed solution theory (IAST) was employed based on the above adsorption results (Supplementary Figs. 32–37). As a result, the predicted selectivity for an equimolar C_2H_2/C_2H_6 (v/v = 50:50) mixture reaches 42 at 273 K and 53 at 298 K (Fig. 4e). In addition, FIR-151 also shows favorable selectivities for CO_2/C_2H_6 (v/v = 50:50; 15 at 273 K and 9 at 298 K (Fig. 4f), outperforming most reported MOPs[46–48]. Furthermore, the structural integrity and permanent porosity of FIR-151 were confirmed by powder X-ray diffraction (PXRD) measurements after gas sorption and the reproducibility of two consecutive BET measurements (Supplementary Fig. 38). These results demonstrate how mechanistic understanding and controlled synthesis of MOPs can yield functional materials[49].

Building on the structural insights of FIR-151, we explored its post-assembly modification potential to tailor material properties (Fig. 5a). Specifically, the replacement of acetate ligands in FIR-151 with methacrylate and benzoate to form FIR-154 and FIR-155, respectively. The successful ligand exchange was verified by ^1H NMR spectroscopy (Supplementary Figs. 39, 40), while the retention of the intact MOP architecture in solution was confirmed by SAXS (Supplementary Figs. 41 and 42). Furthermore, PXRD spectra confirmed the phase purity of the modified MOPs in the solid state (Supplementary Figs. 43 and 44). SCXRD confirmed that both compounds retain the structural integrity of the parental Ti_{24} MOP (Supplementary Table S5). Furthermore, all three MOPs adopt a body-centered cubic close-packed arrangement (Fig. 5b–d). The introduction of benzoate groups in FIR-155 enhances the material's hydrophobicity, as confirmed by contact angle measurements (Supplementary Fig. 45), and facilitates π-π stacking (3.68 Å) between MOPs in its body-centered cubic lattice. Concurrently, the incorporation of methacrylate groups in FIR-154 installs structurally confirmed polymerizable handles, establishing a rational molecular design for exploring chemical functionality tuning and serving as a building block for extended polymeric networks in future studies.

Discussion

In summary, this study significantly advances the field of titanium supramolecular chemistry through the synthesis and structural characterization of FIR-151, a Ti_{24} MOP that exhibits a rare tro topology and represents the highest nuclearity Ti-MOP reported to date. The isolation and structural resolution of two key intermediates, a Ti_{12}

https://doi.org/10.1038/s41467-026-69115-7

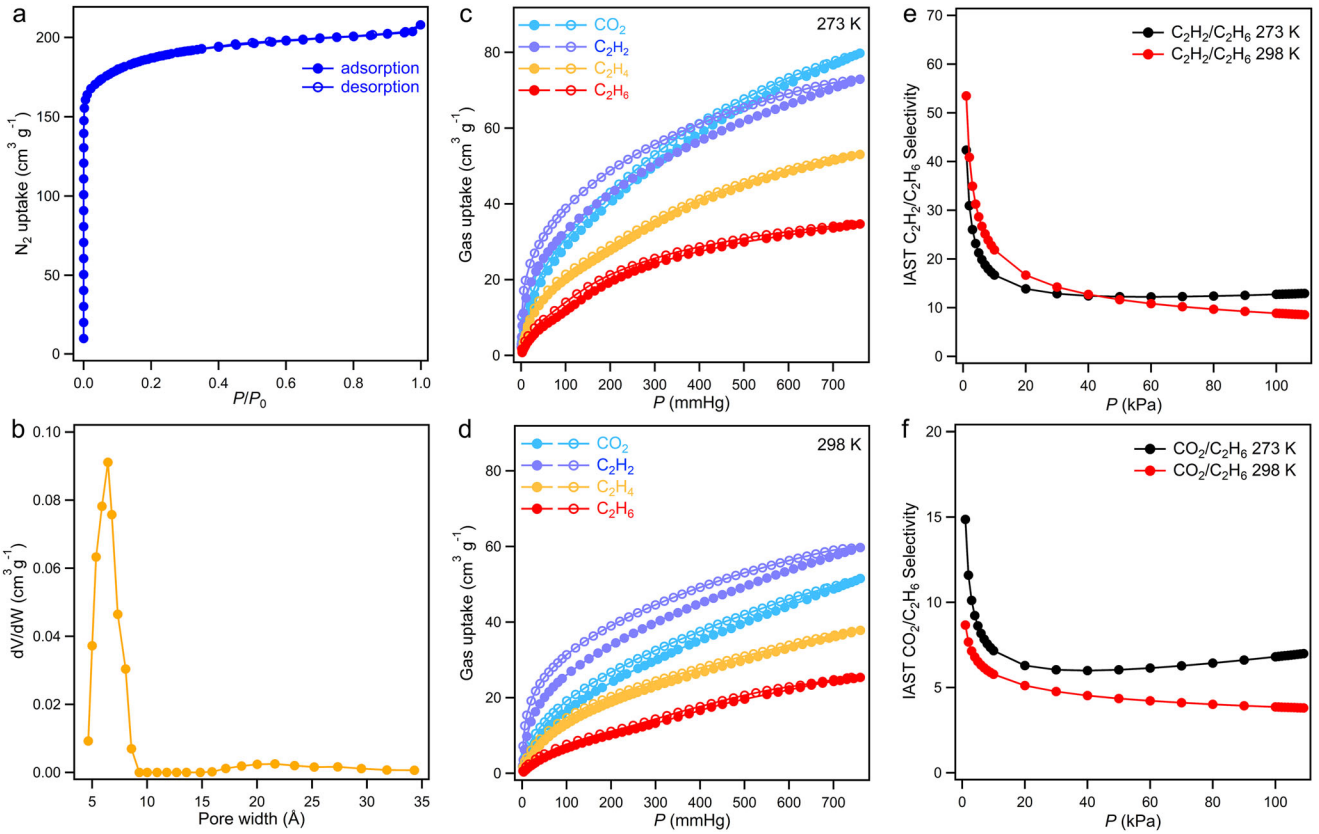

Fig. 4 | Porosity and gas separation selectivity of FIR-151. a N_2-sorption isotherm at 77 K for FIR-151. **b** Pore-size distribution curve of FIR-151 derived from density functional theory (DFT) analysis. **c** The sorption isotherms of FIR-151 for CO_2, C_2H_2, C_2H_4, and C_2H_6 at 273 K. **d** The sorption isotherms of FIR-151 for CO_2, C_2H_2, C_2H_4, and C_2H_6 at 298 K. **e** The IAST selectivities of FIR-151 for C_2H_2/C_2H_6 (50/50, v/v) mixtures at 1 bar. **f** The IAST selectivities of FIR-151 for CO_2/C_2H_6 (50/50, v/v) mixtures at 1 bar. Source data are provided as a Source Data file.

macrocycle in FIR-152 and a Ti_{12} (6-4-6) module in FIR-153, provide critical insight into a hierarchical assembly pathway governed by differential coordination kinetics. FIR-151 demonstrates permanent porosity, selective gas sorption behavior, and post-assembly modification, underscoring its potential as a versatile platform for applied supramolecular science.

By leveraging the inherent reactivity of Ti^{4+} ions through rational pathway engineering, we transform a long-standing synthetic challenge into a strategic advantage for constructing architecturally complex supramolecular systems. This approach establishes an effective strategy for the rational construction of high-nuclearity MOPs, with potential applications in supramolecular synthesis, host-guest chemistry, and functional materials design.

Methods

Synthesis of FIR-151

A mixture of $Ti(O^iPr)_4$ (0.325 mmol, 100 µL), $H_2C_4O_4$ (0.1 mmol, 0.011 g), CH_3CN (4 mL), and CH_3COOH (1 mL) in a 25 mL Teflon-lined stainless-steel autoclave. Then, the mixture was heated at 120 °C for 3 days. After cooling to room temperature, the yellow rhombic dodecahedral crystals were washed with a large amount of CH_3CN, filtered, and stored in CH_3CN (Yield: ~13.1 mg, ca. 22% based on Ti). One of these crystals was used for X-ray crystallography.

Synthesis of FIR-152

A mixture of $Ti(O^iPr)_4$ (0.325 mmol, 100 µL), $NiCl_2{\cdot}6H_2O$ (0.2 mmol, 0.048 g), $H_2C_4O_4$ (0.1 mmol, 0.011 g), CH_3CN (4 mL), and CH_3COOH (1 mL) in a 20 mL vial. Then, the mixture was heated at 80 °C for 7 days. After cooling to room temperature, the yellow block-shaped crystals were washed with CH_3CN and stored in CH_3CN (Yield: ~20.0 mg, ca. 33% based on $H_2C_4O_4$). One of these crystals was used for X-ray crystallography.

Synthesis of FIR-153

A mixture of $Ti(O^iPr)_4$ (0.325 mmol, 100 µL), $NiCl_2{\cdot}6H_2O$ (0.2 mmol, 0.048 g), $H_2C_4O_4$ (0.1 mmol, 0.011 g), tetrabutylammonium bromide (TBAB, 0.2 mmol, 0.062 g), CH_3CN (4 mL), and CH_3COOH (1 mL) in a 20 mL vial. Then, the mixture was heated at 80 °C for 7 days. After cooling to room temperature, the orange hexagonal dipyramid crystals were washed with CH_3CN and stored in CH_3CN (Yield: ~21.2 mg, ca. 35% based on $H_2C_4O_4$). One of these crystals was used for X-ray crystallography.

Synthesis of FIR-154

FIR-151 crystals (0.005 g, 1.154×10^{-6} mol) were dissolved in a DMSO/CH_3CN mixture (v/v = 1/9, 1 mL) under ultrasonication. Methacrylic acid (0.30 mmol, 25 µL) was then added, and the solution was heated at 80 °C for 7 days. After cooling to room temperature, orange crystals of FIR-154 were collected by filtration, washed with CH_3CN, and stored in CH_3CN (Yield: ~5.4 mg, ca. 89% based on FIR-151). One of these crystals was used for X-ray crystallography.

Synthesis of FIR-155

FIR-151 crystals (0.005 g, 1.154×10^{-6} mol) were dissolved in a DMSO/CH_3CN mixture (v/v = 1/9, 1 mL) under ultrasonication. Benzoic acid (0.30 mmol, 0.036 g) was then added, and the solution was heated at 80 °C for 7 days. After cooling to room temperature, yellow single crystals of FIR-155 were collected by filtration, washed with CH_3CN, and stored in CH_3CN (Yield: ~6.5 mg, ca. 86% based on FIR-151). One of these crystals was used for X-ray crystallography.

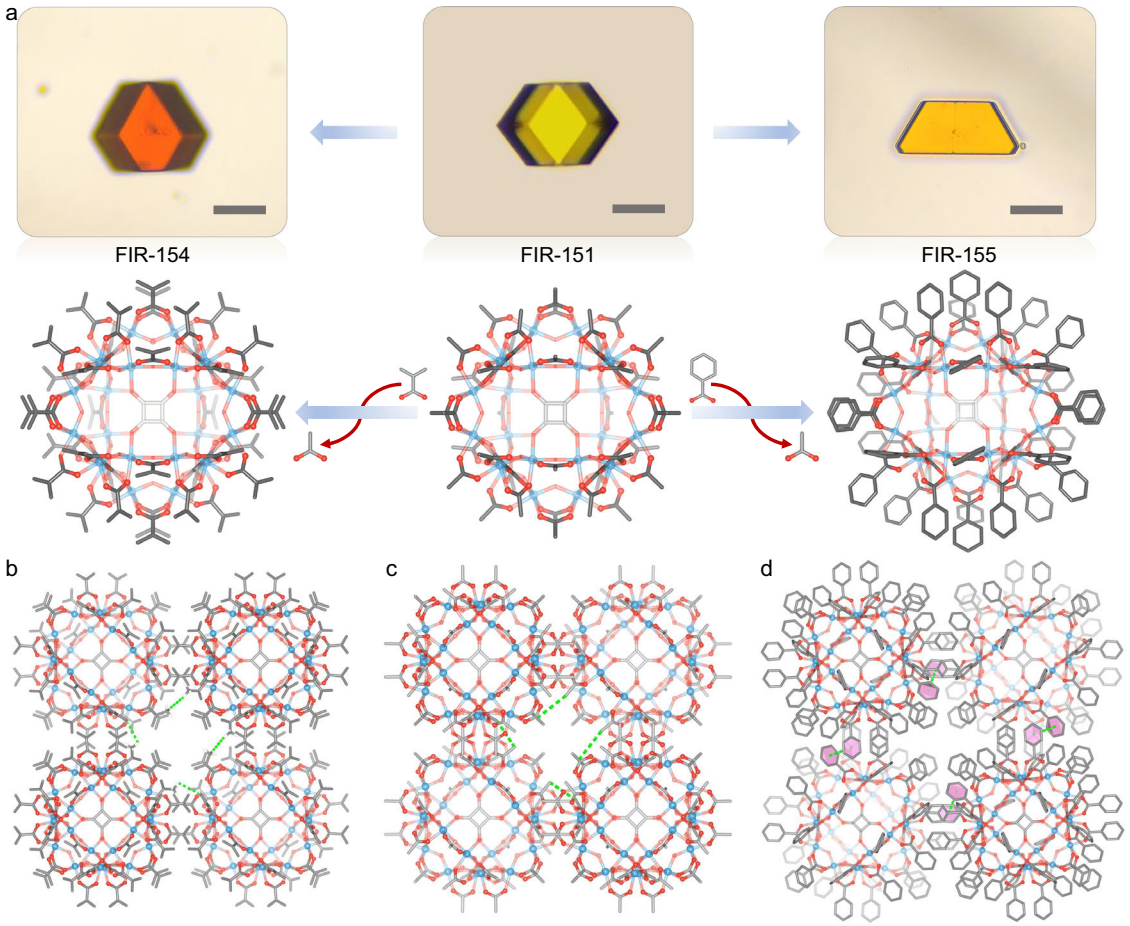

Fig. 5 | Post-assembly modification of Ti_{24} MOPs. a Photographs and schematic of surface ligand exchange on Ti_{24} MOPs, where acetate ligands (CH_3COO^-, FIR-151) are replaced by methacrylic acid (CH_2=C(CH_3)COO^-, FIR-154) and benzoic acid ($C_6H_5COO^-$, FIR-155), scale bar = 50 μm. Crystal packing of modified Ti_{24} MOPs viewed along the *c*-axis: **b** FIR-154, **c** FIR-151, and **d** FIR-155. Atom colors: Ti sky blue, C gray, O red. The green dashed lines indicate hydrogen bonds or π-π interactions between adjacent MOPs.

Solvent exchange and activation of FIR-151

Freshly prepared FIR-151 was soaked in CH_3CN at room temperature for 7 days to exchange the guest CH_3COOH. Subsequently, the samples were activated under dynamic vacuum at 30 °C for 12 h. This temperature ensured the complete removal of the solvents, meanwhile excluding the possibility of FIR-151 decomposition.

Data availability

Crystallographic data for the structures reported in the article have been deposited at the Cambridge Crystallographic Data Centre, under deposition numbers CCDC 2207102 (FIR-151), 2485117 (FIR-152), 2354806 (FIR-153), 2481895 (FIR-154), and 2481896 (FIR-155). Copies of the data can be obtained free of charge via https://www.ccdc.cam.ac.uk/structures/. All other data supporting the findings of this study are included within the paper and its Supplementary Information. Source data are provided with this paper.

References

1. Tranchemontagne, D. J., Ni, Z., O'Keeffe, M. & Yaghi, O. M. Reticular chemistry of metal-organic polyhedra. *Angew. Chem. Int. Ed.* **47**, 5136–5147 (2008).
2. Gosselin, A. J., Rowland, C. A. & Bloch, E. D. Permanently microporous metal-organic polyhedra. *Chem. Rev.* **120**, 8987–9014 (2020).
3. Fang, Y. et al. Catalytic reactions within the cavity of coordination cages. *Chem. Soc. Rev.* **48**, 4707–4730 (2019).
4. Percástegui, E. G., Ronson, T. K. & Nitschke, J. R. Design and applications of water-soluble coordination cages. *Chem. Rev.* **120**, 13480–13544 (2020).
5. Gu, Y. et al. Photoswitching topology in polymer networks with metal-organic cages as crosslinks. *Nature* **560**, 65–69 (2018).
6. Xu, H. et al. A pseudo-cubic metal-organic cage with conformationally switchable faces for dynamically adaptive guest encapsulation. *Nat. Chem.* **17**, 289–296 (2025).
7. Li, Y. et al. Hetero- and homointerlocked metal-organic cages. *J. Am. Chem. Soc.* **146**, 3147–3159 (2024).
8. Chen, J. et al. Unlocking photocycloaddition reactivity of tropolone by cage-confined visible-light photocatalysis for multilevel selective transformation. *J. Am. Chem. Soc.* **146**, 32738–32747 (2024).
9. Ruan, J., Lu, Y.-L., Hu, P. & Su, C.-Y. Asymmetric synthesis of strained multichiral spirocyclobutanes through cage-confined cross [2+2] photocycloaddition. *J. Am. Chem. Soc.* **147**, 10475–10484 (2025).
10. Wang, L. J., Zhang, Z. E., Zhang, Y. Z. & Han, Y. F. Cavity-partitioned self-assembled cage for sequential separation in aqueous solutions. *Angew. Chem. Int. Ed.* **63**, e202407278 (2024).
11. Wang, R. G. et al. In situ cation-switched organometallic cage reconfiguration enables highly selective Li^+ recognition and extraction. *Angew. Chem. Int. Ed.* **64**, e202513692 (2025).
12. Wu, M. X. et al. Dihydrophenazine derived Pd_6L_{12} cage: self-assembly, polyradical cations, and lithium battery cathode application. *Angew. Chem. Int. Ed.* **64**, e202503151 (2025).

13. Yang, Y. et al. Synthesis of covalently linked knotted cage frameworks. *Nat. Synth.* **4**, 1270–1277 (2025).
14. Abe, T., Sanada, N., Takeuchi, K., Okazawa, A. & Hiraoka, S. Assembly of six types of heteroleptic Pd_2L_4 cages under kinetic control. *J. Am. Chem. Soc.* **145**, 28061–28074 (2023).
15. Notheis, M. J., Schnakenburg, G. & von Krbek, L. K. S. Light-driven ratchet mechanism accelerates regioselective metal-cation exchange in a heterobimetallic helicate. *Angew. Chem. Int. Ed.* **64**, e202508952 (2025).
16. Rood, J. A., Boggess, W. C., Noll, B. C. & Henderson, K. W. Assembly of a homochiral, body-centered cubic network composed of vertex-shared Mg_{12} cages: use of electrospray ionization mass spectrometry to monitor metal carboxylate nucleation. *J. Am. Chem. Soc.* **129**, 13675–13682 (2007).
17. Jia, P.-P. et al. Orthogonal self-assembly of a two-step fluorescence-resonance energy transfer system with improved photosensitization efficiency and photooxidation activity. *J. Am. Chem. Soc.* **143**, 399–408 (2020).
18. Gao, M.-Y. et al. Black titanium-oxo clusters with ultralow band gaps and enhanced nonlinear optical performance. *J. Am. Chem. Soc.* **144**, 8153–8161 (2022).
19. Liu, J.-J. et al. Achieving high-efficient photoelectrocatalytic degradation of 4-chlorophenol via functional reformation of titanium-oxo clusters. *J. Am. Chem. Soc.* **145**, 6112–6122 (2023).
20. Schneider, J. et al. Understanding TiO_2 photocatalysis: mechanisms and materials. *Chem. Rev.* **114**, 9919–9986 (2014).
21. Rozes, L. & Sanchez, C. Titanium oxo-clusters: precursors for a Lego-like construction of nanostructured hybrid materials. *Chem. Soc. Rev.* **40**, 1006–1030 (2011).
22. Coppens, P., Chen, Y. & Trzop, E. Crystallography and properties of polyoxotitanate nanoclusters. *Chem. Rev.* **114**, 9645–9661 (2014).
23. Zhu, Q.-Y. & Dai, J. Titanium oxo/alkoxyl clusters anchored with photoactive ligands. *Coord. Chem. Rev.* **430**, 213664 (2021).
24. Zhang, L., Fan, X., Yi, X., Lin, X. & Zhang, J. Coordination-delayed-hydrolysis method for the synthesis and structural modulation of titanium-oxo clusters. *Acc. Chem. Res.* **55**, 3150–3161 (2022).
25. Xie, Y. L., Fang, W. H. & Zhang, J. Aggregation of titanium-oxo clusters. *Aggregate* **5**, e506 (2024).
26. Assi, H., Mouchaham, G., Steunou, N., Devic, T. & Serre, C. Titanium coordination compounds: from discrete metal complexes to metal-organic frameworks. *Chem. Soc. Rev.* **46**, 3431–3452 (2017).
27. Zhu, J., Li, P.-Z., Guo, W., Zhao, Y. & Zou, R. Titanium-based metal-organic frameworks for photocatalytic applications. *Coord. Chem. Rev.* **359**, 80–101 (2018).
28. Yan, Y., Li, C., Wu, Y., Gao, J. & Zhang, Q. From isolated Ti-oxo clusters to infinite Ti-oxo chains and sheets: recent advances in photoactive Ti-based MOFs. *J. Mater. Chem. A* **8**, 15245–15270 (2020).
29. Li, L., Wang, X. S., Liu, T. F. & Ye, J. Titanium-based MOF materials: from crystal engineering to photocatalysis. *Small Methods* **4**, 2000486 (2020).
30. Du, Y., Yan, Q. & Wang, S. Progress and challenges of monometallic titanium coordination polymers. *Small* e2403470 (2024).
31. Scarpi-Luttenauer, M., Mobian, P. & Barloy, L. Synthesis, structure and functions of discrete titanium-based multinuclear architectures. *Coord. Chem. Rev.* **459**, 214439 (2022).
32. Tian, Y.-Q. et al. Ancillary ligand-regulated Ti(IV)-based metallocalixarene coordination cages for photocatalytic H_2 evolution. *Chem. Commun.* **58**, 9034–9037 (2022).
33. Wang, D. et al. Guest modulating the photoactivity of a titanium-oxide cage. *Chem. Sci.* **15**, 19952–19961 (2024).
34. Cui, X. et al. Polyoxotitanate molecular cage featuring four types of ethylenediamines: formation mechanism insight from host-guest interaction and crystallographic study. *Inorg. Chem.* **60**, 9174–9180 (2021).
35. Brückner, C., Powers, R. E. & Raymond, K. N. Symmetry-driven rational design of a tetrahedral supramolecular Ti_4L_4 cluster. *Angew. Chem. Int. Ed.* **37**, 1837–1839 (1998).
36. He, Y. P. et al. Water-soluble and ultrastable Ti_4L_6 tetrahedron with coordination assembly function. *J. Am. Chem. Soc.* **139**, 16845–16851 (2017).
37. Lerma-Berlanga, B. et al. Permanent porosity in hydroxamate titanium-organic polyhedra. *J. Am. Chem. Soc.* **143**, 21195–21199 (2021).
38. Zhu, B. C. et al. Host-guest and photophysical behavior of Ti_8L_{12} cube with encapsulated $[Ti(H_2O)_6]$ species. *Chem. Eur. J.* **24**, 14358–14362 (2018).
39. Gao, M. Y. et al. Fullerene-like polyoxotitanium cage with high solution stability. *J. Am. Chem. Soc.* **138**, 2556–2559 (2016).
40. Chen, G. H. et al. Post-assembly modification of homochiral titanium-organic cages for recognition and separation of molecular isomers. *Angew. Chem. Int. Ed.* **62**, e202300726 (2023).
41. He, Y. P. et al. Combining a titanium-organic cage and a hydrogen-bonded organic cage for highly effective third-order nonlinear optics. *Angew. Chem. Int. Ed.* **60**, 2920–2923 (2020).
42. Zang, H.-Y. et al. Discovery of gigantic molecular nanostructures using a flow reaction array as a search engine. *Nat. Commun.* **5**, 3715 (2014).
43. Salcedo-Abraira, P. et al. A novel porous Ti-squarate as efficient photocatalyst in the overall water splitting reaction under simulated sunlight irradiation. *Adv. Mater.* **33**, 2106627 (2021).
44. Yan, Q. et al. A squarate-pillared titanium oxide quantum sieve towards practical hydrogen isotope separation. *Nat. Commun.* **14**, 4189 (2023).
45. Wyler, R., de Mendoza, J. & Rebek, J. A synthetic cavity assembles through self-complementary hydrogen bonds. *Angew. Chem. Int. Ed* **32**, 1699–1701 (2003).
46. Li, W. et al. Recent advances on porous coordination cages for gas storage and separation. *Coord. Chem. Rev.* **545**, 217032 (2025).
47. Fan, W. et al. Tetrazole-functionalized zirconium metal-organic cages for efficient C_2H_2/C_2H_4 and C_2H_2/CO_2 Separations. *Angew. Chem. Int. Ed* **60**, 17338–17343 (2021).
48. Yang, Z. et al. Packing engineering of zirconium metal-organic cages in mixed matrix membranes for CO_2/CH_4 separation. *Angew. Chem. Int. Ed.* **64**, e202418098 (2025).
49. Troyano, J., Horike, S. & Furukawa, S. Reversible discrete-to-extended metal-organic polyhedra transformation by sulfonic acid surface functionalization. *J. Am. Chem. Soc.* **144**, 19475–19484 (2022).

Acknowledgements

This work was supported by the National Natural Science Foundation of China (Grant Nos. 21935010 (J.Z.), 22571294 (F.W.)) and the Natural Science Foundation of Fujian Province (Grant No. 2022J01505 (F.W.)). The authors thank the staff from BL17B beam-line of the National Facility for Protein Science in Shanghai (NFPS) at Shanghai Synchrotron Radiation Facility for assistance during data collection.

Author contributions

F.W. conceived the project. J.Z. directed the research. H.Z.L. performed experiments associated with molecular synthesis, crystal growth, and gas sorption. C.C. guided the design and drawing of structural diagrams. C.Y.Y. conducted sample collection and basic characterization. F.W. and H.Z.L. wrote the first draft. All authors participated in editing the manuscript.

Competing interests

The authors declare no competing interests.

Additional information

Supplementary information The online version contains supplementary material available at https://doi.org/10.1038/s41467-026-69115-7.

Correspondence and requests for materials should be addressed to Fei Wang or Jian Zhang.

Peer review information *Nature Communications* thanks the anonymous reviewers for their contribution to the peer review of this work. A peer review file is available.